ADVANCES IN ATMOSPHERIC SCIENCES, VOL. 23, NO. 2, 2006, 165–180

Analysis of Ice Water Path Retrieval Errors Over Tropical Ocean

HUANG Jianping* (黄建平)

College of Atmospheric Sciences, Lanzhou University, Lanzhou 730000

(Received 4 February 2005; revised 11 July 2005)

ABSTRACT

Retrieval of multi-layered cloud properties, especially ice water path (IWP), is one of the most perplexing problems in satellite cloud remote sensing. This paper develops a method for improving the IWP retrievals for ice-over-water overlapped cloud systems using Tropical Rainfall Measuring Mission (TRMM) Microwave Imager (TMI) and Visible and Infrared Scanner (VIRS) data. A combined microwave, visible and infrared algorithm is used to identify overlapped clouds and estimate IWP separately from liquid water path. The retrieval error of IWP is then evaluated by comparing the IWP to that retrieved from single-layer ice clouds surrounding the observed overlapping systems. The major IWP retrieval errors of overlapped clouds are primarily controlled by the errors in estimating the visible optical depth. Optical depths are overestimated by about 10–40% due to the influence of the underlying cloud. For the ice-over-warm-water cloud systems (cloud water temperature $T_{\rm w} > 273$ K), the globally averaged IWP retrieval error is about 10%. This cloud type accounts for about 15% of all high-cloud overlapping cases. Ice-over-super-cooled water clouds are the predominant overlapped cloud system, accounting for 55% of the cases. Their global averaged error is ∼17.2%. The largest IWP retrieval error results when ice clouds occur over extremely super-cooled water clouds ($T_{\rm w} \leqslant 255$ K). Overall, roughly 33% of the VIRS IWP retrievals are overestimated due to the effects of the liquid water clouds beneath the cirrus clouds. To improve the accuracy of the IWP retrievals, correction models are developed and applied to all three types of overlapped clouds. The preliminary results indicate that the correction models reduce part of the retrieval error.

Key words: Ice water path, multi-layered cloud, microwave imaging, retrieval errors

doi: 10.1007/s00376-006-0165-4

1. Introduction

Although they are widely recognized to play a critical role in the earth's radiation balance, clouds remain the major source of large uncertainties in climate predictions by general circulation models (GCMs). The difficulties of adequately capturing the cloud radiative effects in GCMs are well documented (Cess et al., 1990). One of the principal reasons for the large uncertainties is the lack of knowledge about cloud overlap. Multi-layered clouds, together with changes in cloud particle size, thermodynamic phase (water or ice) and optical depth, contribute a large part of the cloud-radiation climate feedback (Gupta et al., 1992; Wielicki et al., 1995). Changes in cloud overlap or cloud vertical structure affect the atmospheric general circulation by modifying the distributions of radiative energy and latent heat within the atmosphere (Slingo and Slingo, 1988; Randall et al., 1989; Slingo and Slingo, 1991; Wang and Rossow, 1998).

Climatologically, surface observations show that about 40%–50% of the clouds are multi-layered (Poore et al., 1995; Hahn et al., 1982, 1984; Warren et al., 1985, 1988; Tian and Curry, 1989; Wang et al., 1999, 2000). But when lower clouds are present or during the night when visibility is poor, surface observers may not be able to identify cirrus and altostratus/altocumulus clouds (Poore et al., 1995). Surface observations also do not provide cloud top height/pressure and optical thickness information. Because of the sparse geographical coverage of weather stations, surface observations can only provide the large-scale (15° latitude by 30° longitude over ocean, and 5° by 5° over land; see Hahn et al., 1982, 1984) variation of cloud vertical distributions. With higher spatial and temporal coverage, satellite observations of radiances at solar and infrared wavelengths yield near-global distributions of cloud amount, optical depth, cloud top temperature, and height (Rossow and Schiffer, 1999) as well as effective droplet size (e.g., Han et al., 1994), phase, and ice crystal size (e.g., Minnis et al., 1998). Most remote sensing techniques, however, assume single-layer cloud systems in their retrievals. Multilayered cloud

*E-mail: hjp@lzu.edu.cn

properties are then artificially considered as homogenous single-layer clouds. As such, cloud overlap can cause large errors in the retrievals of many properties including cloud height, optical depth, thermodynamic phase, and particle size. For multi-layered clouds, one of the greatest impediments to accurately determine cloud ice mass for a given atmospheric profile is the influence of underlying liquid water clouds and precipitation on the radiances observed at the top of the atmosphere (TOA). For example, the optical depth derived from a reflected visible radiance represents the combined effects of all cloud layers. Thus, the effects of the liquid water path (LWP) and ice water path (IWP) in multi-layered cloud systems should be separated.

Since reflected solar measurements can be used to retrieve atmospheric total water path (TWP), which includes both cloud water and ice amounts, Lin and Rossow (1996) made the first estimates of global IWP distributions by using a simple separation technique of TWP and cloud LWP retrieved, respectively, by using the International Satellite Cloud and Climatology Project (ISCCP, Rossow and Schiffer, 1999) and from microwave data taken by different satellites. Because of spatial and temporal mismatches between the ISCCP and microwave datasets and uncertainties in both retrievals, the IWP estimates are subject to large errors. Liu and Curry (1998, 1999), Evans et al. (1998), Weng and Grody (2000), and Zhao and Weng (2002) demonstrated the potential for using millimeter-and sub-millimeter-wavelength measurements to directly infer ice cloud properties separately from liquid water clouds. Most of those retrieval algorithms were tested using aircraft *in situ* measurements over tropical oceans or data that was not currently available on satellites.

A variety of methods have been developed to identify multi-layered clouds. Baum et al. (1994) used CO_2 slicing and a spatial coherence method to demonstrate nighttime detection of multi-layered clouds. Jin and Rossow (1997) applied a similar technique for a global analysis of overlapped cloud amounts. Baum and Spinhirne (2000) proposed a 1.6- and 11–μm bispectral threshold method to detect clouds in daylight. The limitation of these techniques is that the optical depth for upper layer ice clouds cannot be large (usually optical depth$<$5). Since satellite microwave measurements at frequencies lower than $\sim$100 GHz are sensitive to water clouds, Lin et al. (1998a, b) used a combination of infrared (IR), visible (VIS), and microwave (MW) data to detect ice clouds overlapping non-precipitating water clouds over water surfaces.

While all of these methods have made progress in solving this stubborn problem, none has been used for continuous and consistent monitoring of multilayered cloud systems. Furthermore, satellite retrievals of multi-layered cloud properties, especially IWP, are still in a development stage and tend to have large uncertainties (e.g., factor of 2 or more). It is clear that retrieval of overlapping clouds from passive instruments such as satellite radiometers is still one of the most perplexing problems in satellite cloud remote sensing and requires additional research.

Recently, Ho et al. (2003) applied the Lin et al.'s (1998a, b) microwave, visible and infrared (MVI) algorithm to combined Tropical Rainfall Measuring Mission (TRMM) Microwave Imager (TMI) and Visible and Infrared Scanner (VIRS) data. Currently, the MVI method is the most feasible approach for retrieving IWP for the overlapped cases. Ho et al. (2003) found that the global mean difference between the TMI liquid water path (LWP_T) and the VIRS liquid water path (LWP_V) is less than 0.01 mm for warm non-precipitating clouds. But for cold clouds, almost 25%–30% of the VIRS total water path (TWP_V) in these cases is actually from liquid water beneath the upper-layer clouds. Thus, the assumption that the cloud is entirely ice when computing VIRS ice water path (IWP_V) introduces some errors in the water path estimations. They suggest that the differences between TWP_V and LWP_T could be used as estimates of IWP. However, the MVI differencing approach to derive IWP in overlapped cases represents only a first step toward constructing an IWP climatology. In reality, the simple differencing of TWP_V and the LWP_T may not provide a correct answer because of differences in the scattering properties of liquid and ice clouds. The uncertainty in the IWP retrieval arises from the TWP_V and LWP_T retrieval errors. Furthermore, the microphysics of the lower cloud may significantly influence the derived optical depth. Thus, the underlying clouds must be properly characterized and the radiative transfer effects of the overlapped cloud system must be taken into account.

In this study, the variability in the IWP is further analyzed using the most recent version of VIRS cloud products and the IWP retrieval error is evaluated for ice-over-water multi-layered cloud systems using collocated VIRS and TMI data. The MVI algorithm (Lin et al., 1998a; Ho et al., 2003) is used to identify the overlapped clouds and estimate IWP values based on VIRS measurements. The IWP values of overlapped clouds are then evaluated by comparing them with the single-layer cirrus clouds surrounding the observed overlapping systems. Correction models are also developed to improve the accuracy of the IWP estimates.

2. Data

The data used in this study are TMI, VIRS measurements taken by the TRMM satellite over open oceans equatorward of 38° latitude. TRMM is in

a 350-km circular orbit with a 35° inclination angle (Kummerow et al., 1998). This orbit produces a sequence of equatorial crossing times that cover the full diurnal cycle in each location within about 46 days. Thus, measurements can be taken over the full range of solar zenith angles over a given tropical region twice per season. TMI is a nine-channel, passive microwave radiometer measuring radiance at frequencies of 10.65, 19.35, 21.3, 37.0 and 85.5 GHz. All channels have both vertically and horizontally polarized measurements except for the 21.3-GHz channel, which has only vertical polarization. TMI scans conically with an incident angle of 52.8° at the sea surface and yields a swath width of about 758.5 km. The 85.5- and 37-GHz effective footprints are 7 km (down-track direction) by 5 km (cross-track direction) and 16 km by 9 km, respectively. The TMI antenna temperatures were converted to brightness temperatures Tb with the method of Wentz (1998). The plane-parallel microwave radiation transfer model (MWRTM) of Lin et al. (1998a) was then used to simulate Tb for all TMI channels. A lookup table (LUT) was built for various atmospheric conditions including an range of cloud temperatures ($T_{\rm w}$), $\rm LWP_T$, atmospheric column water vapor (CWV), near-surface wind speed (WS), and sea surface temperature (SST). For each cloudy TMI pixel, LWP and $T_{\rm w}$ can be retrieved from the LUT simultaneously using SST, WS, CWV, and bias-corrected values of $\rm Tb_{37H}$ and $\rm Tb_{85V}$ (see Fig. 1, Ho et al., 2003). From simulations, Lin et al. (1998a) showed that the simultaneous retrieval yields a bias error of about ±0.01 mm in LWP.

VIRS is a five-channel imager that measures radiances at 0.65, 1.64, 3.75, 10.8, and 12.0 μm with a spatial resolution of about 2 km at nadir view. The VIRS radiance data are used to retrieve cloud fraction, thermodynamic phase (water or ice phase), optical depth, effective particle size, water path (WP), cloud-top temperature $T_{\rm c}$, and cloud top height z for the Clouds and Earth's Radiant Energy System (CERES) project (Minnis et al., 1995). Because of the time limitation of the CERES TRMM project, this study only analyzes the TRMM data from 1 January to 31 August 1998. The VIRS cross-track scan yields coverage roughly between 38°N and 38°S. VIRS ice and liquid water path ($\rm IWP_V$ and $\rm LWP_V$) retrievals are calculated from the cloud optical depth and effective particle size estimated from visible and near-infrared wavelengths (Minnis et al., 1995, 1998) assuming a monotonic cloud thermodynamic phase of the whole atmospheric column.

The CERES TRMM Edition-2 VIRS cloud properties and spectral radiances (Minnis et al., 2002) are used here. Ho et al. (2003) used the CERES TRMM Edition-1 cloud property dataset (Minnis et al., 1999). In addition to other changes, the Edition-2 algorithm uses a different visible channel reflectance parameterization (Arduini et al., 2002) and accounts for absorption of visible wavelength radiation by water vapor. Relative to the Edition-1 retrievals, these two changes tend to reduce the optical depth for thin clouds, increase the optical depth for thicker clouds, and minimize the solar zenith angle dependence of the optical depth retrievals.

To estimate the properties of overlapping nonprecipitating clouds over oceans, the VIRS pixel-level radiances and cloud properties were collocated with TMI measurements. Since TMI has much larger footprints than VIRS, the VIRS cloud products were convolved with TMI measurements to produce equivalent VIRS cloud retrievals within the TMI footprints. Only the TMI pixels containing more than 15% cloudiness from the convolved VIRS-TMI data are used here. The resulting dataset constitutes 81.6% of all TMI pixels taken over the oceans. Because TMI and VIRS are on the same spacecraft, the temporal and spatial mismatches of VIRS and TMI measurements are negligible. The detailed collocation and retrieval processes for the TRMM data have been reported by Ho et al. (2003).

3. Identification and variability of multilayered clouds

The value of $T_{\rm w}$ retrieved from TMI data represents a mean cloud temperature for an integrated cloud column whereas $T_{\rm c}$ derived from the VIRS data represents the temperature near the top of the cloud for optically thick clouds (Minnis et al., 1995). Therefore, when the difference, $\Delta T_{wc} = T_{\rm w} - T_{\rm c}$, is significantly positive, it is likely that the observed system consists of overlapped clouds (Lin et al., 1998b; Ho et al., 2003). In this study, three special overcast groups are selected and analyzed. The conditions for selecting these three groups are: (1) single-layer high ice clouds (ICLD: 100% ice phase, $T_{\rm w} > 290$ K, $T_{\rm c} < 273$ K, $|T_{\rm s} - T_{\rm w}| < 3$ K and $T_{\rm s} - T_{\rm c} > 36$ K, where $T_{\rm s}$ represents SST), (2) overlapped clouds (OCLD: 100% ice phase, $T_{\rm w} < 290$ K, $T_{\rm c} < 273$ K, $T_{\rm w} - T_{\rm c} > 15$ K, and $T_{\rm s} - T_{\rm c} > 36$ K), and (3) single-layer low warm water clouds (WCLD: 100% water phase, 273 K$< T_{\rm w} <$ 290 K, $T_{\rm w} - T_{\rm c} < 5$ K and $T_{\rm s} - T_{\rm c} > 10$ K). The criteria used here are similar to that used by Ho et al. (2003). The thermodynamic (ice or water) phase of the highest cloud was determined by the VIRS analysis. The thresholds used here exclude some overcast cloud data. Thus, the classification does not assign all overcast clouds into one of the three groups since only high-ice-over-water clouds are the focus of this study. The three-group total constitutes about 18% of all overcast cases. Individual ICLD, OCLD, and WCLD systems account for 36.4%, 48.2%, and 15.4%

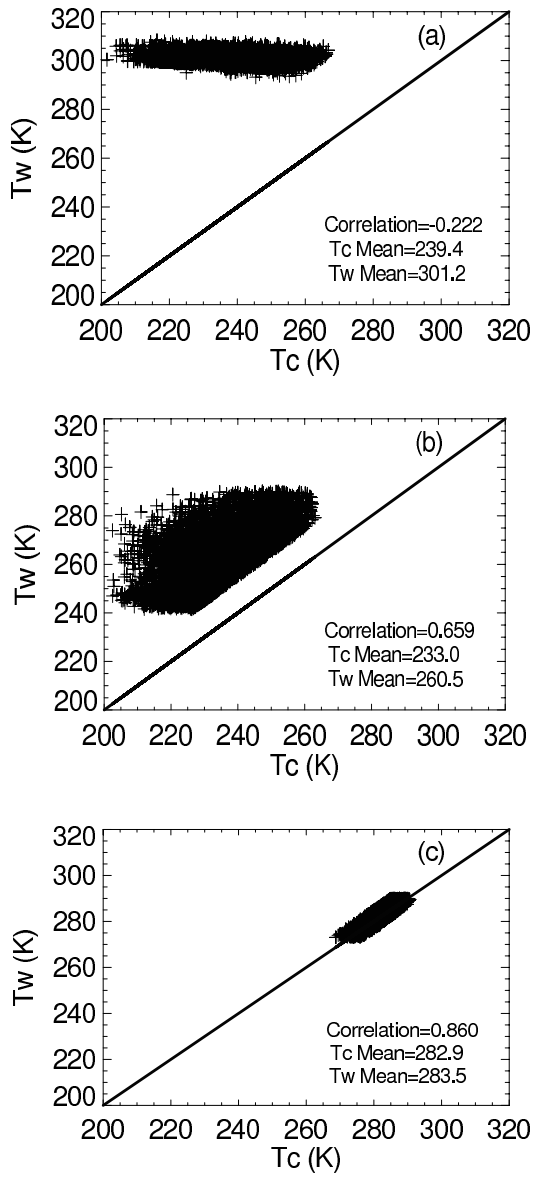

Fig. 1. Comparison of TMI T_w with VIRS T_c over global tropical ocean for (a) ICLD, (b) OCLD and (c) WCLD for July 1998.

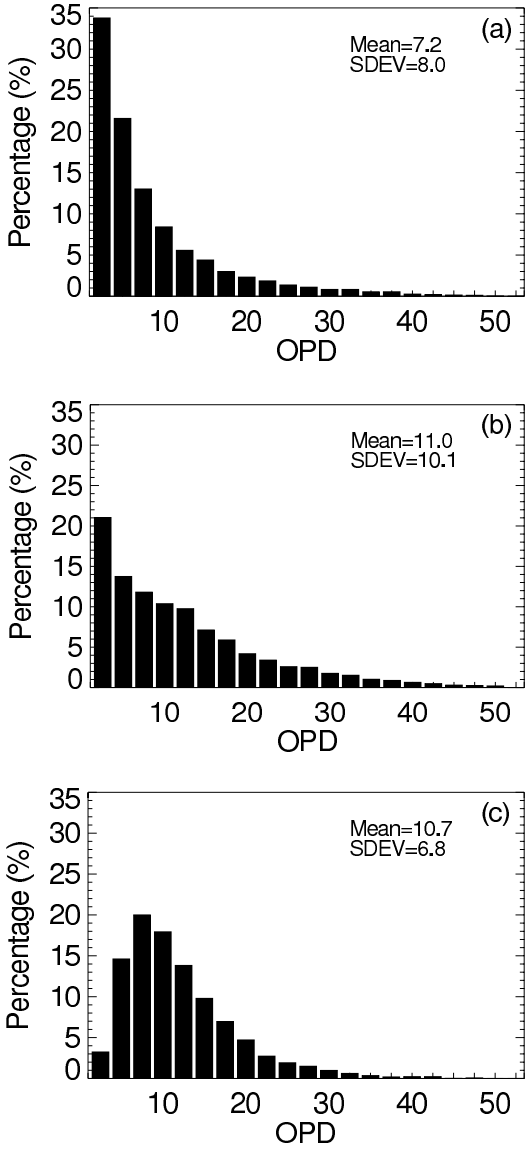

Fig. 2. Histogram of VIRS optical depth (OPD) over global tropical ocean for (a) ICLD, (b) OCLD and (c) WCLD for July 1998.

of the total overlapped cloud systems, respectively. The corresponding seasonal variabilities around the mean frequencies of the three cloud systems are about 8.5%, 4.5% and 6.3%, respectively.

Figure 1 shows the scatter plot of T_w with T_c for each of the three groups for tropical ocean (20°S–20°N) regions during July 1998. The relationships between T_w and T_c are distinct for each group. For single-layer ICLD in Fig. 1a, T_w is very narrowly distributed around 300 K. In contrast, T_c is very low, ranging from 210 to 265 K with means near 239.4 K and a standard deviation of about 12.1 K. It should be emphasized that, in the ICLD case, there is almost no cloud water in the atmosphere (LWP_T values are near zero), and the TMI radiances are directly from the sea surface with some attenuation by atmospheric water vapor and other trace gases. Thus, the estimated T_w values do not really represent cloud water temperatures; instead, they are closely related to SST. The negative linear correlation coefficient (R=−0.22) between T_w and T_c further demonstrates a relationship between T_w and SST. As SST increases, the convection tends to deepen, and more cirrus clouds occur at higher altitudes. The OCLD systems have a different correlation between T_w and T_c (Fig. 1b). T_w averages about 27.5 K greater than T_c (233 K), although the standard deviations, 11.3 K and 12.5 K, respectively,

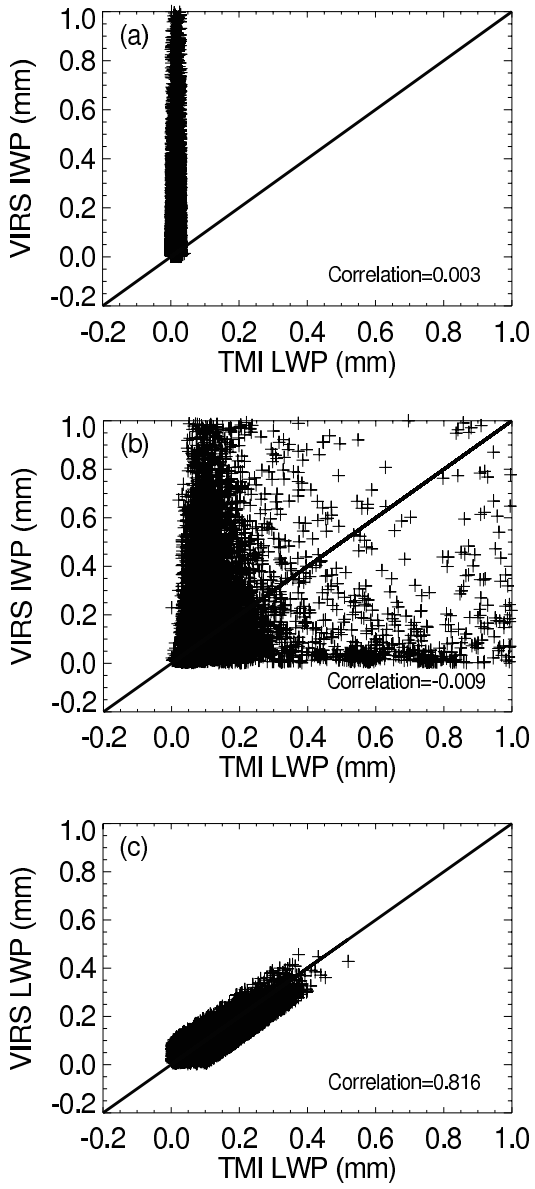

Fig. 3. Comparison of VIRS IWP or LWP with TMI LWP over global tropical ocean for (a) ICLD, (b) OCLD and (c) WCLD for July 1998.

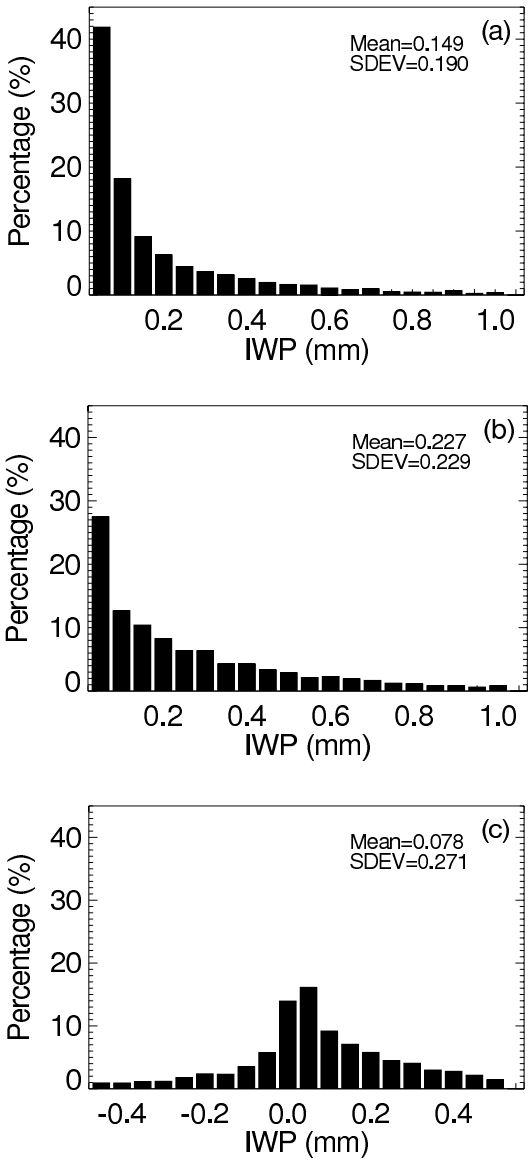

Fig. 4. Histogram of VIRS IWP over global tropical ocean for (a) ICLD and (b) OCLD, and (c) the difference between OCLD and ICLD, for July 1998.

are similar. In addition to the presence of overlapped clouds, this large difference arises from the fact that the TMI-measured microwave radiation emanates from much lower cloud layers than the IR radiances measured by VIRS. The cloud temperature T_w is more or less a column-averaged value of cloud liquid water temperature as opposed to the near-cloud-top temperature (T_c) retrieved from the VIRS data. For the low WCLD, T_w is strongly and positively correlated with T_c(R=0.86; Fig. 1c) at a statistical significance level above 99%. The mean difference between the two estimates is very small, less than 1 K, suggesting that the temperature differences between the cloud base and the cloud top of low level water clouds are likely to be only within 1 K corresponding to cloud thickness of several hundred meters. This result confirms that significant differences between T_w and T_c can be used as the critical condition for identifying cloud overlap.

Figure 2 shows frequency distributions of VIRS optical depth (OPD) for all three cloud groups for July 1998. The single-layer ice cloud optical depths (Fig. 2a) are about 35% less than the overlapped cloud values (Fig. 2b), possibly indicating the effect of lower-level water clouds on the retrieved optical depth. The mean WCLD optical depth (Fig. 2c) is nearly equal to that for OCLD, but the similarity ends there. The

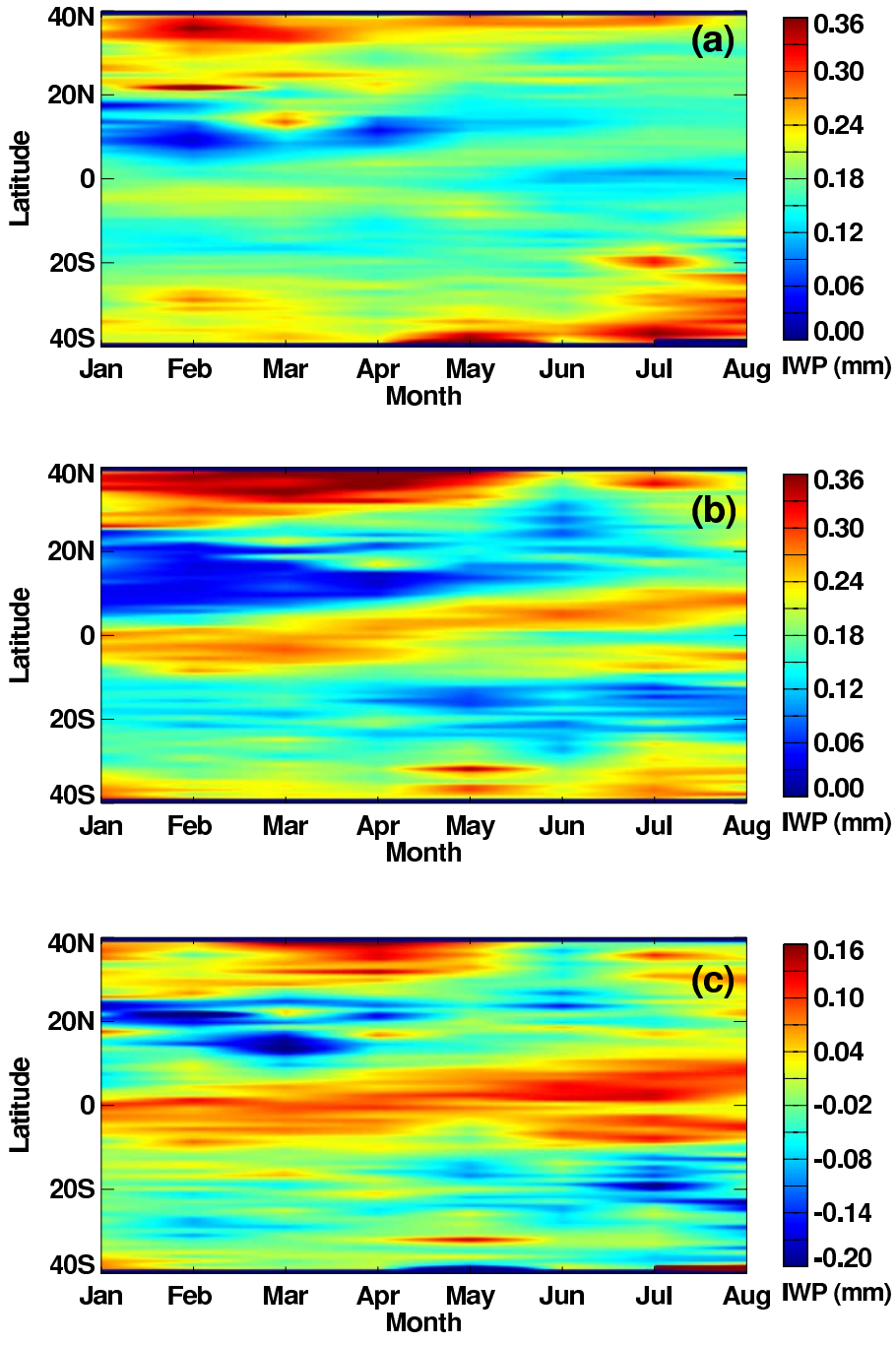

Fig. 5. Seasonal variation of monthly zonal mean VIRS IWP for (a) ICLD and (b) OCLD, and (c) the difference between OCLD and ICLD, from January to August 1998.

shapes of the histograms and standard deviations (SDEVs) are much different. The frequency distribution of the OCLD optical depths appears to be intermediate between ICLD and WCLD and the OCLD standard deviation is much greater than those for the WCLD and ICLD. For ICLD, optical depths less than 8 occur more than 70% of the time compared to only 46% for overlapped cloud systems. For single-layer water clouds, the optical depths are concentrated between 7 and 12 (56%).

To illustrate the effect of overlapped clouds on VIRS IWP (IWP_V), Fig. 3 shows the scatter plots of

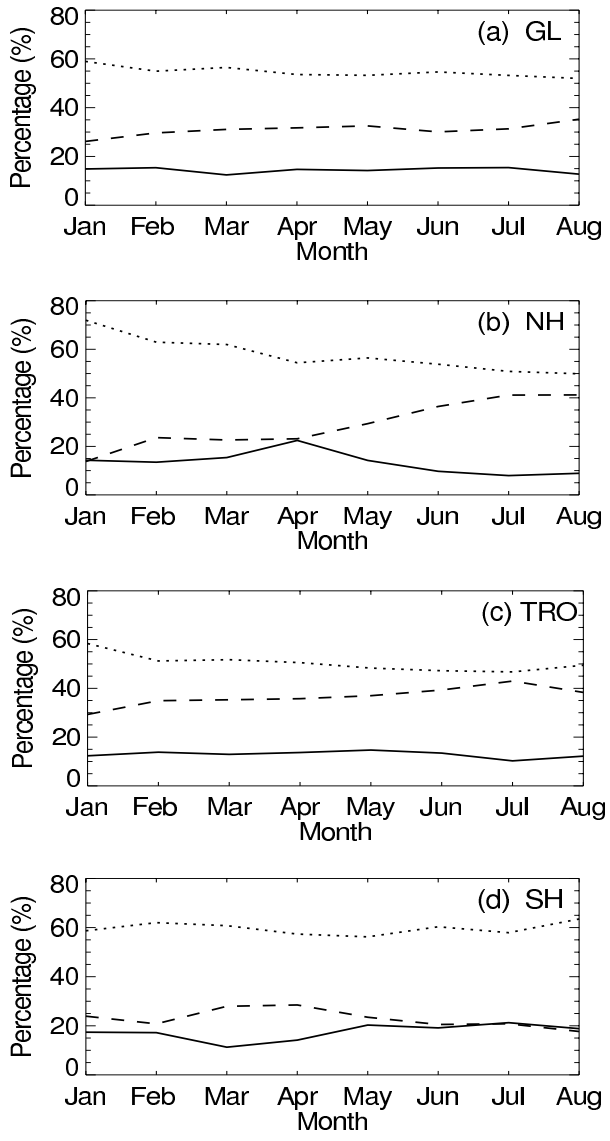

Fig. 6. Seasonal variation of occurrence frequency of three different overlapped cloud systems globally (GL) and in different latitudinal bands (NH: Northern Hemisphere; TRO: Tropical Ocean; SH; Southern Hemisphere) from January to August 1998. Solid curves are for IOWW, dashed curves for IOSW, and long-dashed curves for IOEW.

IWP_V or LWP_V with LWP_T for each cloud group in tropical ocean (20°S–20°N) areas for July 1998. As expected, almost no correlation exists between IWP_V and LWP_T in either the ICLD or OCLD cases. IWP_V varies from 0 to 1.0 mm and is vertically narrowly distributed around LWP_T=0 in the ICLD case (Fig. 3a), while there is a large spread for overlapped systems (Fig. 3b). Figure 3c shows coincident LWP_V and LWP_T retrievals for WCLD. The cloud systems in this category are dominated by stratocumulus clouds with minimal contamination by thin cirrus clouds. The two LWP estimates are well correlated (0.816) with a mean difference, $LWP_V - LWP_T$, of −0.017 mm and a standard deviation of 0.01 mm. The correlation is much better than that found using the Edition-1 data, but the mean Edition-2 VIRS value underestimates the TMI values by 15% compared to a 6% overestimate in the Edition-1 data (Ho et al., 2003). The July 1998 differences represent the worst case. For all 8 months, the mean Edition-2 LWP_V is only 2% less than the mean LWP_T. Therefore, the VIRS and TMI liquid water path values are very consistent overall.

One means for quantifying the impact of the underlying water clouds on the VIRS retrieval of IWP is to compare nearly adjacent TMI pixels filled with overcast ice clouds. One pixel should contain measurable amounts of LWP while the other should be free of liquid water. The IWP_V distributions for a set of 500 pairs of tropical OCLD pixels and the nearest ICLD pixels observed during July 1998 are shown in Figs. 4a and 4b. The respective IWP_V histograms are similar to the optical depth histograms in Figs. 2a and 2b. Nearly 60% of the ICLD values are less than 0.1 mm compared to only 40% for the OCLD pixels. Although the mean OCLD IWP_V is 0.078-mm greater than its ICLD counterpart for these cases, the ICLD IWP_V does not always exceed IWP_V from its nearest OCLD neighbor as indicated in the difference distribution in Fig. 4c. The larger OCLD IWP_V values could be due to either more deeply developed ice clouds in overlapped fields or to a significant contribution of the LWP in the lower-level clouds to total reflectance and, hence, to the IWP_V values. In the latter case, the IWP_V values more or less represent column total water path and, theoretically, can be corrected using LWP_T. If the former case predominates, then few negative values would be expected in Fig. 4c because it implies that the IWP in the multilayered clouds should always exceed IWP in the single-layer conditions. If LWP were the dominant factor and the ice clouds are somewhat randomly distributed over the water clouds, then the probability for observing a negative difference will increase. That is, some thin cirrus clouds would occur over a thin water cloud and some thick cirrus clouds would occur over water-cloud-free areas. Given that 22% of the OCLD-ICLD differences in Fig. 4c are negative, it appears that the underlying LWP is the predominant factor causing the differences in IWP_V between single-layer and multi-layered clouds. It should be noted that denser ice clouds may form coincidentally with liquid water clouds, but these systems are frequently precipitating resulting in their exclusion from this analysis. Clouds are defined as precipitating if the values of Tb_{37V}-Tb_{37H} are less than 37 K (Lin and Rossow, 1994). The precipitation clouds were excluded when TMI retrieval was matched with

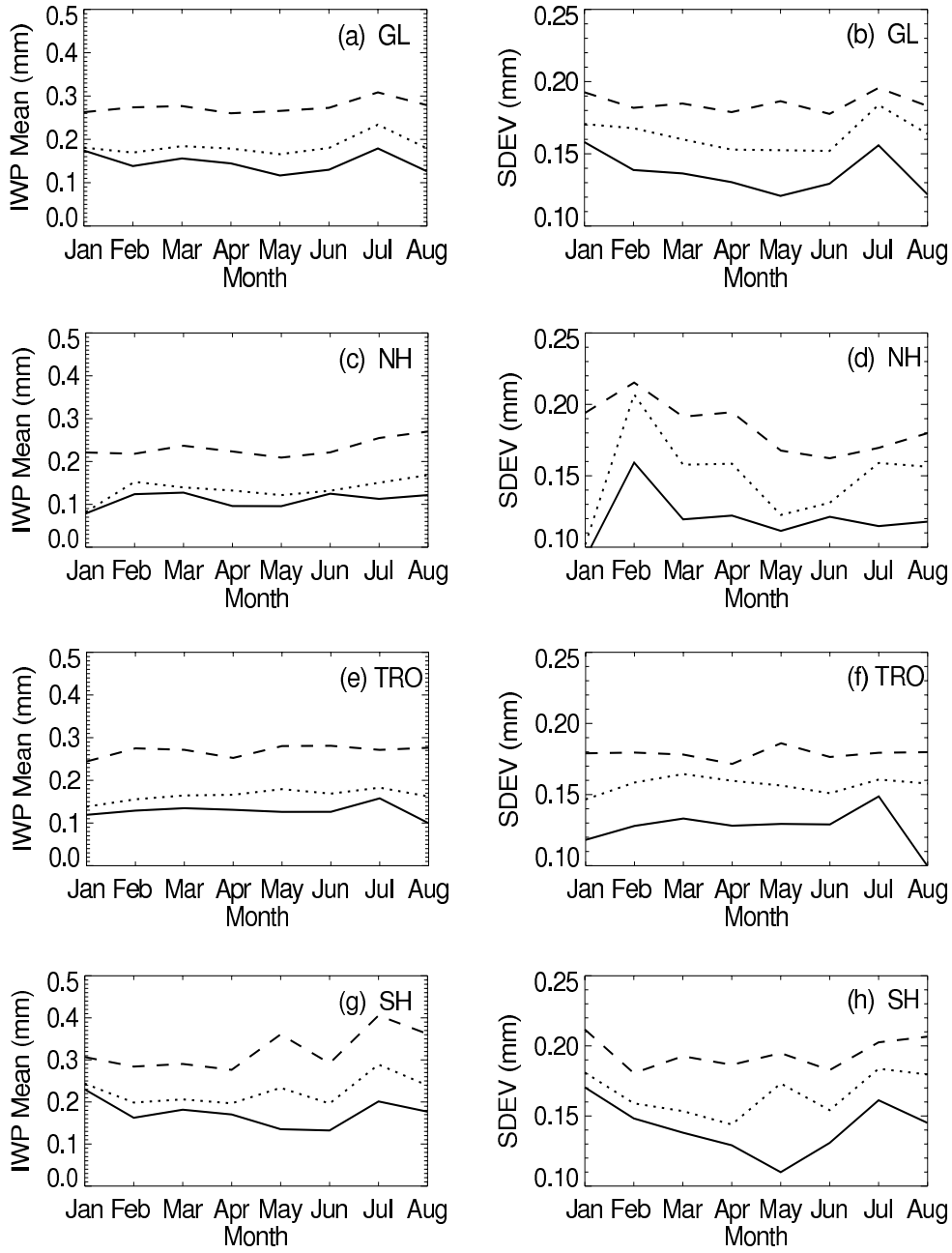

Fig. 7. Seasonal variation of regional mean (left panels) and standard deviation (SDEV, right panels) of IWP for: IOWW (solid curves); IOSW (dashed curves) and IOEW (long-dashed curves) from January to August 1998.

VIRS (Ho et al., 2003).

Figures 5a and b show the monthly and zonal variations of mean IWP_V for ICLD and OCLD, respectively. These monthly zonal means are averaged only when overcast ice clouds are detected. For single-layer ice clouds (Fig. 5a), both the largest values and strongest seasonal variability are found in the mid latitudes of both hemispheres. The mid-latitude seasonal variations in multi-layer cloud mean IWP_V are similar but not as pronounced. During the winter seasons in the respective hemispheres, cold fronts at those latitudes generate thicker cirrus clouds than for other seasons and locations. The OCLD IWP_V values up to 0.4 mm are also found approximately during the springtime. A relative maximum in the OCLD IWP_V follows the northward shift of the inter-tropical convergence

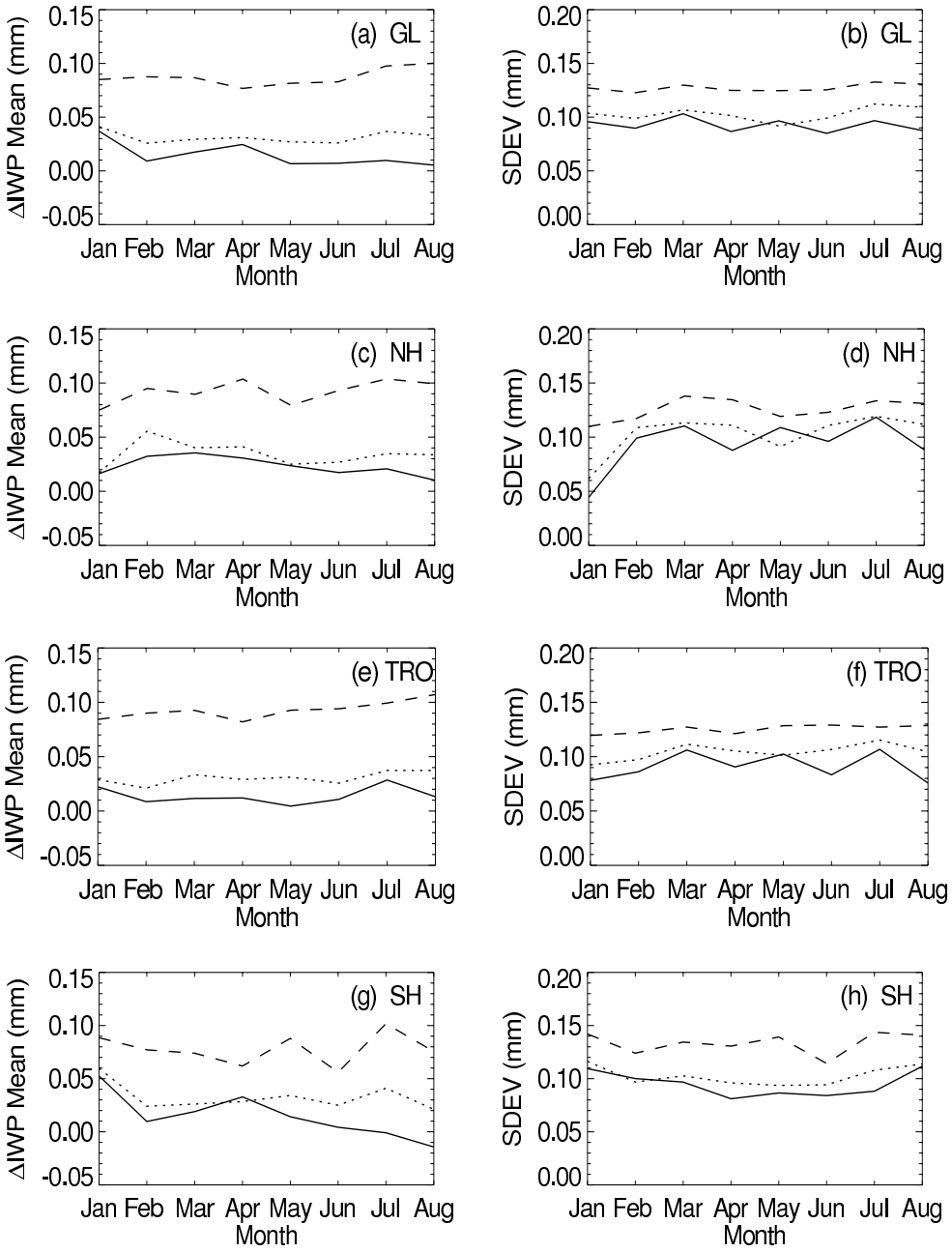

Fig. 8. Seasonal variation of regional mean (left panels) and standard deviation (SDEV, right panels) of ΔIWP for: IOWW (solid curves); IOSW (dashed curves) and IOEW (long-dashed curves) from January to August 1998.

zone (ITCZ) from March through August. The major systematic IWP_V differences between overlapped and single-layer ice clouds occur in the tropical regions for all seasons (Fig. 5c) where both thin cirrus and thick anvil clouds generated by tropical deep convection are frequently observed. Surprisingly, the ICLD IWP_V in the southern mid latitudes is generally equal to or less than the OCLD mean, especially in the austral winter.

4. Evaluation of ice water path retrieval

To further evaluate the influence of underlying clouds on the IWP retrieval, the OCLD data are separated into three categories based on the value of T_w. These three types of clouds include: (1) ice-over-warm-water cloud systems (IOWW) for which $T_w > 273$ K; (2) ice-over-supercooled water cloud systems (IOSW)

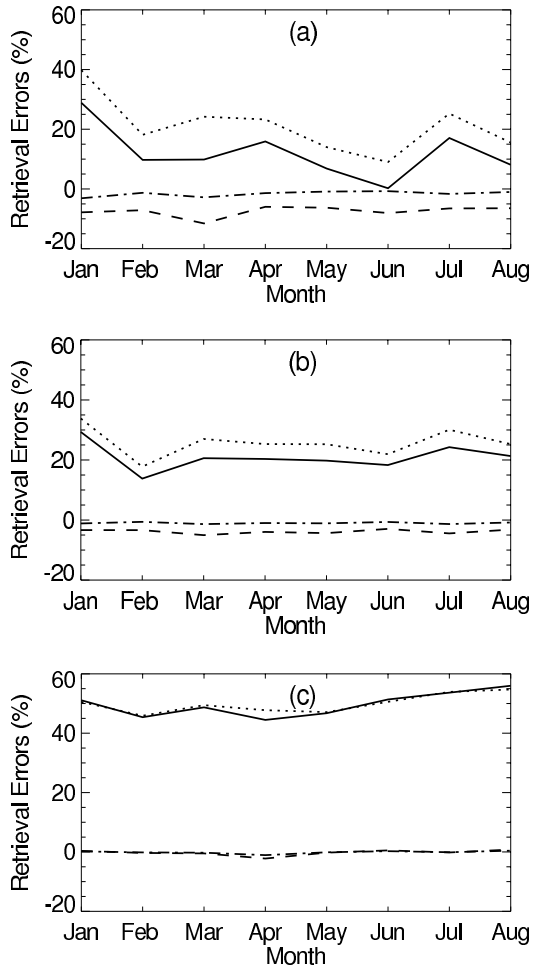

Fig. 9. Seasonal variation of retrieval errors over global ocean for (a) IOWW, (b) IOSW and (c) IOEW. The solid curves are for the $\Delta\Theta/\Theta_V$ term, dashed curves for the $\Delta\tau/\tau$ term, long-dashed for retrieval errors due to the effective diameter term, and the dotted-long-dashed curves are for the nonlinear interaction term in Eq. (2).

having 255 K$< T_w <$ 273 K; and (3) ice-over-extreme-supercooled water clouds (IOEW) with $T_w <$ 255 K. The 255 K is an empirical parameter based on statistical analysis (Bin Ling, private communication, 2005). For IOSW and IOEW, the lower-layer clouds may consist of a mixture of both ice and water particles while both thin cirrus and thick anvils can comprise the upper-layer clouds. The deepest convective clouds are likely to be confined to the IOEW category.

Figure 6 shows the occurrence frequency variations for the three overlapped cloud types in different zonal bands from January through August 1998. The occurrence frequency is defined as the percentage of the overlap type relative to the total number of OCLD pixels. The IOSW clouds (dotted curves) are the major type of the ice-over-water cloud systems in all regions. The globally averaged IOSW frequency accounts for more than 55% of all OCLD pixels compared to 15% and 30% for IOEW (dashed curves) and IOWW (solid curves), respectively. These results are consistent with ship observations (Hahn et al., 1982), which show that in the Tropics, cirrus clouds overlap altostratus, cumulus and cumulonimbus more often than they occur over stratus and stratocumulus. Globally (GL, between 38°N and 38°S), the occurrences of the three overlap types vary minimally with season (Fig. 6a). IOEW increases by ∼8% while IOSW decreases by a similar amount from January to August. The most striking seasonal changes occur between 20°N and 38°N (NH, Fig. 6b), where IOSW drops by 20% as IOEW increases by 25% from winter to summer. The IOWW peaks in April and reaches a minimum during summer. Presumably, the seasonal rise in IOEW is linked to the increase in deep convection, which would raise liquid water up to greater altitudes underneath anvil cirrus than the less vigorous baroclinic disturbances that produce many layers of water clouds beneath the cirrus shields. A similar convergence of the IOSW and IOEW occurs in the Tropics (TRO, Fig. 6c) during the boreal summer when the ITCZ is more developed. The seasonal variability in the three overlap types is least in the southern midlatitudes (SH, Fig. 6d) where IOEW and IOWW are of the same magnitude.

The instantaneous uncertainty in $\mathrm{LWP_T}$ is on the order of 0.04 mm. To reduce the uncertainties (∼0.04 mm) in the microwave $\mathrm{LWP_T}$ retrievals, the 1° gridded averages are considered in the following study. Figure 7 shows the seasonal changes of regional means (left panels) and standard deviations (right panels) of gridded $\mathrm{IWP_V}$ for the three kinds of overlapped clouds. The IOEW clouds hold the highest amounts of ice water path with the strongest variability, followed by the IOSW systems. In the tropical region, the mean (Fig. 7e) and standard deviation (Fig. 7f) of IOEW clouds are about 0.27 mm and 0.18 mm, respectively, while for IOSW systems, the values are smaller and about 0.16 mm and 0.15 mm, respectively.

Since there are no proper observational data to validate the retrieval errors of $\mathrm{IWP_V}$, the differences of IWP_V between OCLD and ICLD can be, in the first order, considered as relative retrieval bias errors of IWP_V of OCLD, that is,

$$\Delta\Theta(t, r_o) = \Theta_{\mathrm{OCLD}}(t, r_o) - \Theta_{\mathrm{ICLD}}(t, r_s)\,, \quad (1)$$

where Θ is the IWP, t is the time, and r_o and r_s are the location of grids of OCLD and ICLD of the surrounding area, respectively. $\mathrm{IWP_{OCLD}}$ (Θ_{OCLD}) represents the $\mathrm{IWP_V}$ values of OCLD, while $\mathrm{IWP_{ICLD}}$ (Θ_{ICLD}) is for the $\mathrm{IWP_V}$ values of non-overlapped single layer ice clouds of neighboring upper layer ice clouds of overlapped clouds. The non-overlapped single layer ICLD grids are defined as those grids that co-exist with the OCLD grids in the small region (10° by 10°) at the

same time. Obviously, the assumption is not valid for tropical convective systems since the cirrus parts of the clouds often have less ice amount than the thick anvils that are close to the convective cores and frequently have both ice and super-cooled water layers. However, it is usually acceptable under the conditions of extended tropical cirrus sheets where upper level ice clouds are not correlated with lower layer water clouds. Seasonal changes of mean (left panels) and standard deviation (SDEV, right panels) of ΔIWP for these three categories of clouds are depicted in Fig. 8. The mean and standard deviation of ΔIWP for IOEW clouds (long-dashed curves in Fig. 8) are much higher than those of IOSW (dashed curves) and IOWW (solid curves) in all regions and months. For example, the globally averaged ΔIWP values of IOEW and IOWW are around 0.087 mm and 0.014 mm, respectively. In other words, the $\mathrm{IWP_V}$ of OCLD, in global average, is about 0.087 mm greater than $\mathrm{IWP_V}$ of single layer cloud surrounding IOEW systems.

As discussed by Minnis et al. (1998), IWP_V is a function of visible optical depth (τ) and ice particle effective diameter (D_e), that is,

$$\Theta_{\mathrm{V}} = \tau(a_1 D_{\mathrm{e}} + a_2 D_{\mathrm{e}}^2 + a_3 D_{\mathrm{e}}^3)\,.$$

The percent of retrieval bias errors due to the underlying water cloud can be derived as:

$$\frac{\Delta\Theta}{\Theta_{\mathrm{V}}} = \frac{\Delta\tau}{\tau} + F_D(D_{\mathrm{e}}, \Delta D_{\mathrm{e}})\frac{\Delta D_{\mathrm{e}}}{D_{\mathrm{e}}} + F_D(D_{\mathrm{e}}, \Delta D_{\mathrm{e}})\frac{\Delta D_{\mathrm{e}}}{D_{\mathrm{e}}}\frac{\Delta\tau}{\tau}\,, \qquad (2)$$

where

$$F_D(D_{\mathrm{e}}, \Delta D_{\mathrm{e}}) = \frac{a_1 + a_2(\Delta D_{\mathrm{e}} + 2D_{\mathrm{e}}) + a_3(\Delta D_{\mathrm{e}}^2 + 3\Delta D_{\mathrm{e}} D_{\mathrm{e}} + 3D_{\mathrm{e}}^2)}{a_1 + a_2 D_{\mathrm{e}} + a_3 D_{\mathrm{e}}^2}\,,$$

Θ is the IWP, and a_i ($i = 1, 2$, and 3) are constant coefficients (Minnis et al., 1998). From Eq. (2), the bias error of $\mathrm{IWP_V}$ is linearly related to the bias error of optical depth but nonlinearly to the uncertainties in diameter. The IWP error is directly proportional to the error of the optical depth. The IWP error increases as the optical depth varies from its true value. The error characteristics are also modified slightly by the particle effective size. Figure 9 shows the seasonal variations of the relative retrieval bias error (in %) of the three types of overlapped clouds over global oceans from January to August 1998. The solid curves are for the $\Delta\Theta/\Theta_{\mathrm{V}}$ term, dashed curves are for the $\Delta\tau/\tau$ term, and long dashed curves are for retrieval errors of the second term in Eq. (2) due to the effective diameter. The dotted long dashed curves are for the third term in Eq. (2) which represent the nonlinear interaction between $\Delta\tau$ and ΔD_e. Here $\Delta\tau$ and ΔD_e are the difference between OCLD and ICLD obtained by using Eq. (1). As expected, the ice over extreme

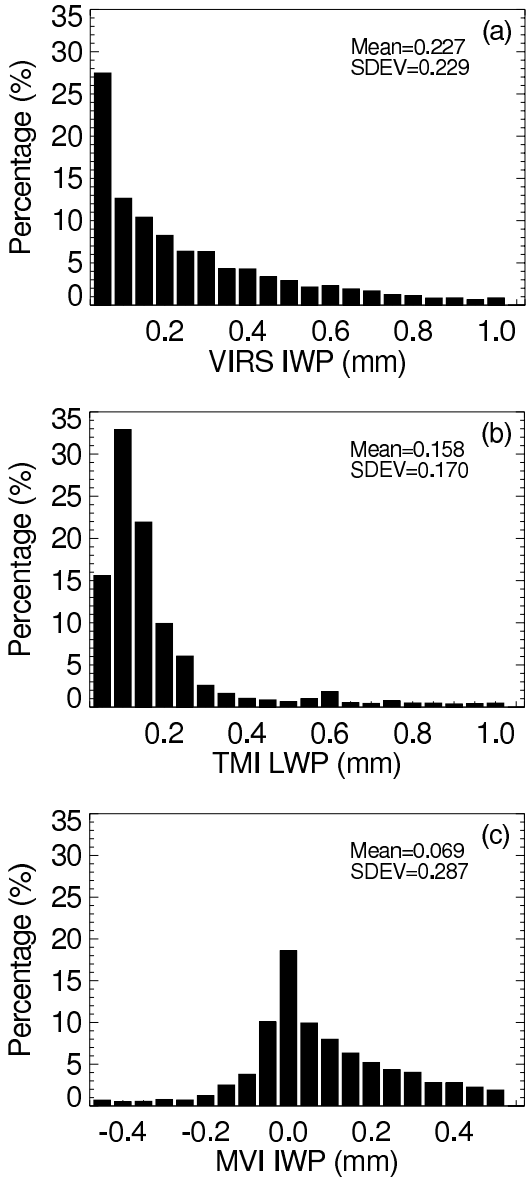

Fig. 10. Histogram of (a) VIRS IWP, (b) TMI LWP, and (c) MVI IWP over global tropical ocean for July 1998.

super-cooled water clouds (IOEW) holds the largest retrieval bias errors. The eight-month average is about 49.68%. This means that almost 49.68% of $\mathrm{IWP_V}$ in the IOEW systems is actually from super-cooled liquid water clouds beneath the upper layer ice clouds. For the IOWW and IOSW cases, however, the retrieval errors are significant less than the IOEW, and the eight-month mean values of $\Delta\Theta/\Theta_{\mathrm{V}}$ are 12.08% and 20.97% in these respective cases. But the seasonal variability of retrieval error is very strong in the IOWW system. This may be due to the IOWW system being often associated with fronts in the wintertime in extra-tropical regions. As also shown in Figs. 9b and 9c, the bias errors of retrieved $\mathrm{IWP_V}$ are primarily controlled by the

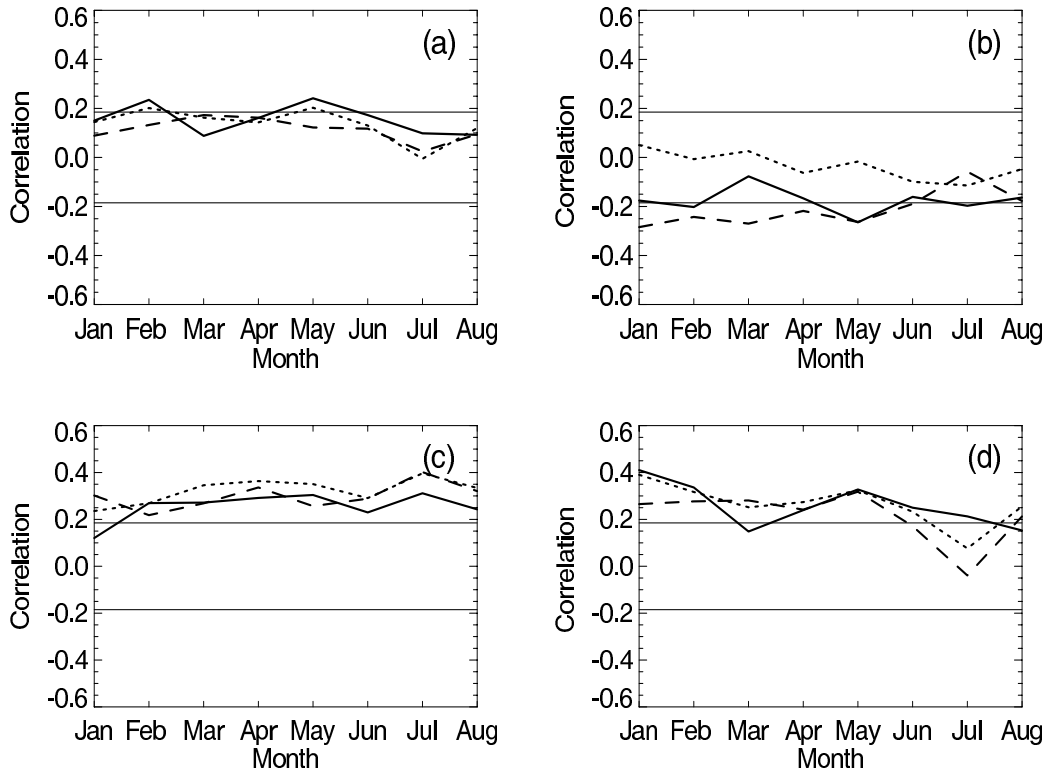

Fig. 11. Seasonal variation of correlation between ΔIWP and (a) TMI LWP, (b) TMI T_w, (c) wind speed, and (d) water vapor for IOWW (solid curves); IOSW (dashed curves) and IOEW (long-dashed curves).

inconsistency in the estimated optical depths over ICDL and OCLD clouds for the ice-over-cold-water cloud in the IOSW and IOEW cases. It is shown that the error of IWP_V apparently increases linearly as the difference of optical depth increases. The effect of effective diameter on the IWP_V retrieval is a small balance term in Eq. (2), which indicates the statistical averages of the effective ice particle size for single and multiple layer ice clouds are about the same as long as these clouds do not have significant precipitation for ice-over-cold-water cloud. But for ice-over-warm-water cloud (Fig. 9a), optical depth and diameter are significant contributions to the bias error of IWP_V. The eight-month mean $\Delta\tau/\tau$ for IOWW (Fig. 9a) is around 21.16%, which is about 9% greater than the bias error of $\Delta\Theta/\Theta_V$. The average value of the D_e term [second term in Eq. (2)] is −7.8%. The difference could be due to the impact of the underlying water cloud reflectance on the total 3.7-μm radiance used to retrieve D_e, if the ice cloud is optically thin (Kawamoto et al., 2002). Most IOWW clouds are optical thin cirrus cloud over lower warm water cloud. If the optical depth of the ice cloud exceeds 4 or 5, then D_e should be unaffected by the lower cloud. The similarities in D_e between the IOSW and IOEW overlapped cases and the single-layered clouds suggest that there is no distinct difference in D_e between the single-layered ice cloud and the multilayered clouds. It should be emphasized that the retrieval errors discussed here are the relative error caused by underlying cloud. Other errors are assumed to be canceled in calculating the IWP difference between OCLD and ICLD.

5. Development of correction model

As mentioned above, VIRS IWP represents the total column water amount; a better IWP estimate can be calculated from the difference between VIRS IWP_V and TMI LWP_T, i.e.,

$$\Theta_{TV} = \Theta_V - \Theta_T ,$$

where Θ is the IWP, and Θ_{TV} (IWP_{TV}) is defined as the MVI IWP by Ho et al. (2003). Figure 10 compares the frequency distributions of VIRS IWP_V, TMI LWP_T and the MVI IWP_{TV}. It should be emphasized that VIRS IWP_V actually represents the total WP for 100% overcast ice phase clouds. As shown in Fig. 10, the IWP values obtained from MVI are considerably different from the original VIRS estimates. The mean MVI IWP_V is around 0.069 mm (Fig. 10c), while the

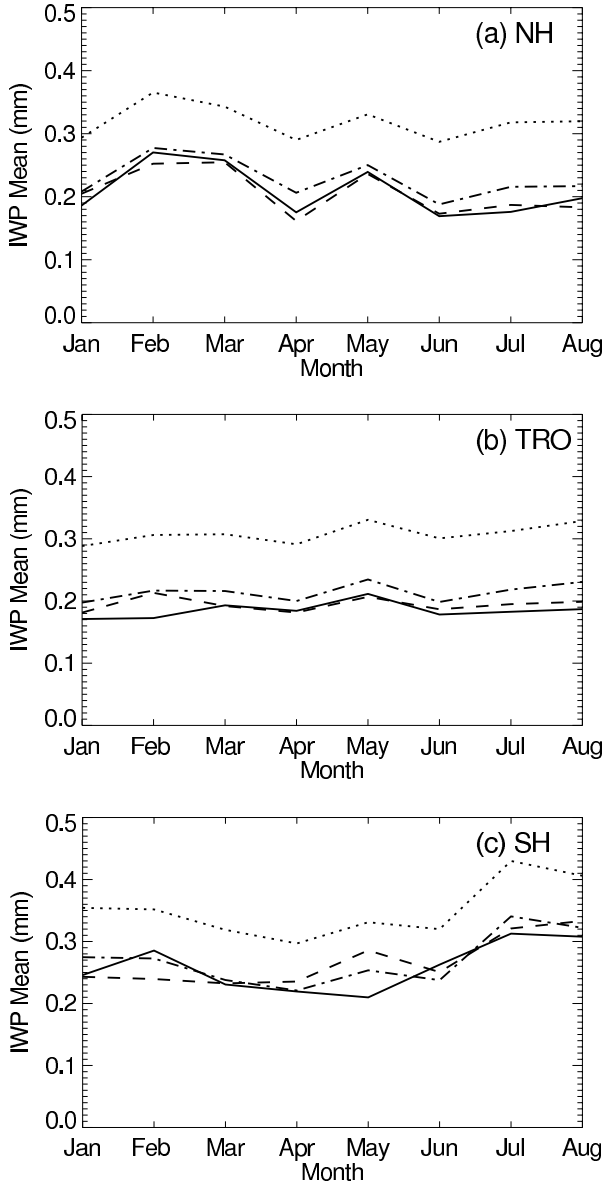

Fig. 12. Comparison of corrected IWP (solid curves) with original IWP (dashed curves), IWP of surrounding ICLD (long-dashed curves) and MVI IWP (dotted-long-dashed curves) for an IOEW system for (a) Northern Hemisphere (NH), (b) Tropical Ocean (TRO) and (c) Southern Hemisphere (SH) from January to August 1998.

mean VIRS $\mathrm{IWP_V}$ is around 0.227 (Fig. 10a). However, some $\mathrm{IWP_{TV}}$ values are negative. Cloud pixels with negative $\mathrm{IWP_{TV}}$ values are mainly due to the impact of the large $\mathrm{LWP_T}$ of the lower level water clouds. When lower layer water clouds are drizzling or contain large particles, the visible and near-IR techniques may underestimate the LWP values for the portion of the overlapped systems. (Lin et al., 1998b; Gerber, 1996; Masunaga et al., 2002). For very large LWP (>0.4 mm) cases, or the cases with IWP_{TV} significantly less than zero shown in Fig. 10c, the satellite visible measurements can be even saturated and produce significant smaller WP values compared with MW estimations (Lin and Rossow, 1994; Liu et al., 1995). The results indicate that the simple differencing of total $\mathrm{WP_V}$ (or $\mathrm{IWP_V}$ for 100% ice phase) and the TMI $\mathrm{LWP_T}$ may not provide a correct answer because of the differences in the scattering properties of liquid and ice clouds. Furthermore, the microphysics of the lower cloud may significantly influence the derived optical depth.

To further examine the effect of lower level water cloud on upper layer ice cloud retrieval, Fig. 11 shows correlation coefficients between ΔIWP and TMI $\mathrm{LWP_T}, T_\mathrm{w}$, near sea surface wind speed and water vapor. The solid curves represent the correlation coefficient between IOWW, while the dashed and long-dashed curves are for the IOSW and IOEW cases, respectively. The thin straight lines indicate the 95% significance level. For IOSW and IOEW, the correlation coefficient between ΔIWP and $\mathrm{LWP_T}$ is close to the 95% significance level for most months except for June-July-August (Fig. 11a). But for IOWW, there is no significant response in all months except for February and May (Fig. 11a). There is a slightly negative correlation between ΔIWP and T_w for IOEW clouds in the early months of the year. For the other cases and the IOSW overlapped systems, the relationships are weak (Fig. 11b) because high clouds do not have a very good temperature relationship to the underlying liquid water layers (Tian and Curry, 1989; Lin et al., 1998b; Ho et al., 2003). The correlation coefficient between ΔIWP and wind speed and water vapor, however, are statistically significant for most months for all three overlapped clouds (Figs. 11c and d). The significant ΔIWP dependences on wind speed and water vapor are caused by large-scale dynamics and thermodynamics. Near-sea-surface winds, especially the wind convergence, are one of the major driving forces for convection and high cloud formation. Water vapor values represent the potential available amounts of moisture for convection to generate upper layer clouds. Strong winds and high boundary layer water vapor amounts usually can generate and/or are associated with strong convection activities, which produce great vertical extension of tropical high clouds and cause large IWP. Similar results are found in VIRS optical depth τ (figure not shown).

Based on the results mentioned above, we can develop an $\mathrm{IWP_V}$ correction model for reducing the effect of lower level clouds on the upper level ice cloud retrievals. The correction model should include the VIRS optical depth τ, TMI cloud liquid water temperature T_w, TMI liquid water path $\mathrm{LWP_T}$, TMI surface

wind speed and the water vapor. For any time and region, the general correction can be written as:

$$\begin{aligned}\Delta\Theta(t,r) =&\zeta(\tau)\{C_0(t,r)+\\ &C_1(t,r)T_{\rm w}+C_2(t,r){\rm LWP_T}+\\ &C_3(t,r)W_{\rm s}+C_4(t,r)W_{\rm v}\}\,,\end{aligned}\tag{4}$$

where

$$\zeta(\tau)=\frac{e^{\tau}-e^{-\tau}}{e^{\tau}+e^{-\tau}}\,,$$

where Θ is the IWP, and t and r are the time and location, respectively. The first term in Eq. (4) represents the controlling of optical depth. When τ is less than 8, the correction should be very small. The coefficients, $C_i(t,r)$ $(i=0,\ldots,4)$ are computed using a least squares multiple regression fit for each month and region. The final corrected $\rm IWP_V$ of OCLD can be expressed as:

$$\Theta_{\rm corrected}(t,r)=\Theta_{\rm original}(t,r)-\Delta\Theta(t,r)\,.\tag{5}$$

As shown in Eqs. (4) and (5), the correction model is actually a modification of the MVI differencing method for introducing more information of the lower level water cloud. If C_0, C_1, C_3 and C_4 are equal to zero, $\zeta(\tau)=C_4=1$, then Eq. (5) becomes the same as Eq. (3).

For the gridded data with $\rm IWP_{TV}$ larger than zero, we have randomly selected half of these data as the historical dataset to determine the regression coefficients and to build the lookup table. The resulting coefficients, then, are used to predict the $\Delta{\rm IWP}(t,r)$ by using Eq. (3) and to correct the IWP values with Eq. (4) for the other half of the gridded data. To demonstrate the capability of the correction models, Fig. 12 shows the comparisons among corrected $\rm IWP_V$, original $\rm IWP_V$, the surrounding single layer cloud $\rm IWP_V$, and MVI $\rm IWP_{TV}$ for the IOEW case over the three different regions from January to August 1998. As shown in Fig. 12, both the corrected $\rm IWP_V$ (solid curves) and MVI $\rm IWP_{TV}$ (dotted-long-dashed curves) are significantly different from the original $\rm IWP_V$ (dashed curves) and are close to the $\rm IWP_V$ of the surrounding single layer ICLD (long dashed curves). The original $\rm IWP_V$ values are overestimated by more than 30%. It is clear that these correction models can significantly reduce the retrieval error and produce more reasonable $\rm IWP_V$ values for multi-layered cloud systems due to their introduction of more information of underlying cloud and circulation conditions from TMI measurements. Of course, these results are preliminary and more tests need to be done. Although it is very hard to judge how good the correction methods are compared to the MVI technique at the present stage of IWP estimations due to the lack of large scale and long term *in situ* measurements, one of the advantages of using a correction model is that it saves computational time in collocation and will be fast in operations. The disadvantage is that the correction method statistically adjusts the IWP values of overlapped systems to be consistent with neighboring single layer ice clouds. For baroclinic frontal systems, the ice water amounts may significantly vary with neighboring locations. Thus, the current method may underestimate or overestimate the IWP values due to small corrections when compared with the neighboring full ice phased thick anvil or thin cirrus clouds, as mentioned before.

6. Conclusions and discussion

Global information on ice water path in ice clouds is urgently needed for testing global climate models and other applications. A better understanding of IWP and its large-scale distribution is important to climate research for improving our ability to parameterize and validate cloud/precipitation processes in global climate models. But satellite retrievals of IWP are still in the developing stage and tend to have large uncertainties (e.g., a factor of 2 or more). Recently developed, the MVI technique (Lin et al., 1998a, b) shows promise for improving the determination of cloud overlap for optically thick cases over ocean.

A basic framework and some examples of the determination of ice water path in multi-layered cloud systems are provided in this paper. It has demonstrated the capabilities of the MVI method for deriving a variety of cloud properties, including identification of multilayered cloud systems. Cloud properties for both single layer ice and water clouds were compared with multilayered cloud systems for different climatological regions. For multi-layered cloud systems, $T_{\rm c}$ is about 27.5 K colder than $T_{\rm w}$, indicating that high ice clouds and low liquid-water clouds are well detected by the VIRS and TMI methods, respectively. The significant difference between $T_{\rm w}$ and $T_{\rm c}$ can be used as the critical condition for identifying the cloud overlapping. The mean $\rm IWP_V$ of OCLD is generally about 0.065 mm higher than that of ICLD in the Tropics. The larger $\rm IWP_V$ value of OCLD is the result of the more extended vertical structure of overlapped high clouds than of single layer high clouds. The major systematic $\rm IWP_V$ differences between OCLD and single layer ICLD occur in the tropical regions for all seasons where both thin cirrus and thick anvil clouds generated by tropical deep convection are frequently observed.

The MVI cloud products can also be used to analyze the error of $\rm IWP_V$ and develop the correction model. The results show that the accuracy of the $\rm IWP_V$ in multi-layered clouds depends on the vertical structure of the multi-layered clouds. On average, the major retrieval error of the IWP of overlapped cloud

is primarily controlled by the errors in estimating the visible optical depth. The optical depth values are overestimated by about 10%–40% due to the influence of the underlying cloud. For the ice over warm water cloud systems ($T_w > 273$ K), the globally averaged retrieval error of IWP is about 10%. The occurrence frequency of this cloud is about 15% of the total high cloud overlapping cases. The systems with ice over supercooled water clouds (255 K$< T_w <$ 273 K) are the major components of overlapped cloud systems with a 55% occurrence frequency. Their globally averaged error is about 17.24%. The largest retrieval error of IWP is from the multilayer clouds with ice over extreme supercooled water cloud ($T_w \leqslant 255$ K). About 33% of VIRS IWP values are overestimated due to the effects of the lower layer liquid water clouds beneath the upper layer cirrus clouds.

To improve the accuracy of the IWP estimation, the correction models were developed and applied to all three types of overlapped clouds. The preliminary result indicate that the correction models significantly reduce the retrieval errors and produce more reasonable IWP values. The major limitation of the correction models is that these models are purely statistical and it is not possible to distinguish between physical and random relationships in the data. The representativeness of the IWP values of neighboring clouds with respect to those of the overlapped systems needs further investigation. Also, the models may be biased by the sampling of the TRMM satellite. More satellite data and ground observations must be used to test the correction models. Furthermore, the current correction models are only available for the ice over water cloud systems; more studies on other types of overlapping systems are needed.

Acknowledgments. The author would like to thank Alice Fan and Sunny Sun-Mack for their help in data processing. Thanks also go to Drs. P. Minnis and B. Lin for reviewing this paper and giving many helpful comments. The TRMM data were provided by the Distributed Active Archive Center at the NASA Goddard Space Flight Center, Greenbelt, Maryland.

REFERENCES

Arduini, R. F., P. Minnis, and D. F. Young, 2002: Investigation of a visible reflectance parameterization for determining cloud properties in multi-layered clouds. Proc. 11th AMS Conf. Cloud Physics., Ogden, UT, June 3–7, CD-ROM, P2.4.

Baum, B. A., and J. D. Spinhirne, 2000: Remote sensing of cloud properties using MODIS airborne simulator imagery during SUCCESS, 3. Cloud overlap. *J. Geophys, Res.,* **105**, 11793–11804.

Baum, B. A., R. F. Arduini, B. A. Weilicki, P. Minnis, and S. C. Tsay, 1994: Multilevel cloud retrieval using multispectral HIRS and AVHRR data: Nighttime oceanic analysis. *J. Geophys. Res.,* **99**, 5499–5514.

Cess, R. D., and Coauthors, 1990: Intercomparison and interpretation of climate feedback process in 19 atmospheric general circulation models. *J. Geophys. Res.*, **95**, 16601–16615.

Committee on Earth and Environmental Sciences (CEES), 1990: Our Changing Planet: The FY 1991 Research Plan of the U. S. Global Change Research Program, U. S. Geol. Surv., White House Printing Office, Washington, D. C., 253pp.

Dong, X., P. Minnis, G. G. Mace, W. L. Smith, Jr., M. Poellot, R. T. Marchand, and A. D. Rapp, 2002: Comparison of stratus cloud properties deduced from surface, GOES, and aircraft data during the March 2000 ARM Cloud IOP. *J. Atmos. Sci.*, **59**, 3256–3284.

Evans, K. F., S. J. Walter, A. J. Heymsfield, and M. N. Deeter, 1998: Modeling of submillimeter passive remote sensing of cirrus clouds. *J. Appl. Meteor.*, **37**, 184–205.

Gupta, S. K., W. L. Darnell, and A. C. Wilber, 1992: A parameterization for surface longwave radiation from satellite data: Recent improvements. *J. Appl. Meteor.*, **31**, 1361–1367.

Hahn, C. J., S. G. Warren, J. Gordon, R. M. Chervin, and R. Jenne, 1982: Atlas of simultaneous occurrence of different cloud types over ocean. NCAR Tech. Note, TN-201 + STR, 212pp.

Hahn, C. J., S. G. Warren, J. Gordon, R. M. Chervin, and R. Jenne, 1984: Atlas of simultaneous occurrence of different cloud types over land. NCAR Tech. Note, TN-241 + STR, 211pp.

Han, Q., W. B. Rossow, and A. A. Lacis, 1994: Near-global survey of effective droplet radii in liquid water clouds using ISCCP data. *J. Climate*, **7**, 465–497.

Ho, S.-P., B. Lin, P. Minnis, and T.-F. Fan, 2003: Estimation of cloud vertical structure and water amount over tropical oceans using VIRS and TMI data, *J. Geophyhs. Res.*, **108**(D14), 4419, doi: 10.1029/2002JD003298.

Jin, Y., and W. B. Rossow, 1997: Detection of cirrus overlapping low-level cloud. *J. Geophys. Res.*, **102**, 1727–1737.

Kawamoto, K., P. Minnis, W. L. Smith Jr., and A. D. Rapp, 2002: Detecting multilayer clouds using satellite solar and IR channels. *Proc. 11th AMS Conf. Cloud Physics., Ogden*, UT, June 3–7, CD-ROM, JP1.18.

Kummerow, C., W. Barnes, T. Kozu, J. Shiue, and J. Simpson, 1998: The Tropical Rainfall Measuring Mission (TRMM) sensor package. *J. Atmos. Oceanic Technol.*, **15**, 809–817.

Lin, B., and W. B. Rossow, 1996: Seasonal variation of liquid and ice water path in non-precipitating clouds over oceans. *J. Climate*, **9**, 2890–2902.

Lin, B., B. Wielicki, P. Minnis, and W. Rossow, 1998a: Estimation of water cloud properties from satellite microwave, infrared and visible measurements in oceanic environments, I: microwave brightness temperature simulations. *J. Geophys. Res.*, **103**, 3873–3886.

Lin, B., P. Minnis, B. Wielicki, D. R. Doelling, R. Palikonda, D. F. Young, and T. Uttal, 1998b: Estimation of water cloud properties from satellite microwave, infrared and visible measurements in oceanic environments, II: Results. *J. Geophys. Res.*, **103**, 3887–3905.

Lin, B., P. Minnis, A. Fan, J. A. Curry, and H. Gerber, 2001: Comparison of cloud liquid water paths derived from *in situ* and microwave radiometer data taken during the SHEBA/FIREACE. *Geophys. Res. Lett.*, **28**, 975–978.

Liu, G., and J. A. Curry, 1998: Remote sensing of ice water characteristics in tropical clouds using aircraft microwave data. *J. Appl. Meteor.*, **37**, 337–355.

Liu, G., and J. A. Curry, 1999: Tropical ice water amount and its relations to other atmospheric hydrological parameters as inferred from satellite data. *J. Appl. Meteor.*, **38**, 1182–1194.

Masunaga, H., T. Y. Nakajima, T. Nakajima, M. Kachi, R. Oki, and S. Kuroda, 2002: Physical properties of maritime low clouds as retrieved by combined use of Tropical Rainfall Measurement Mission Microwave Imager and Visible/Infrared Scanner: Algorithm. *J. Geophys. Res.*, **107**(D10), 4083, doi:10.1029/2001JD000743.

Minnis, P., and Coauthors, 1995: Cloud Optical Property Retrieval (Subsystem 4.3). "Clouds and the Earth's Radiant Energy System (CERES) Algorithm Theoretical Basis Document, Volume III: Cloud Analyses and Radiance Inversions (Subsystem 4)", NASA RP 1376 Vol. 3, CERES Science Team, Ed., 135–176.

Minnis, P., D. P. Garber, D. F. Young, R. F. Arduini, and Y. Takano, 1998: Parameterization of reflectance and effective emittance for satellite remote sensing of cloud properties. *J. Atmos. Sci.*, **55**, 3313–3339.

Minnis, P., D. F. Young, B. A. Wielicki, P. W. Heck, S. Sun-Mack, and T. D. Murray, 1999: Cloud properties derived from VIRS for CERES. *Proc. AMS 10th Conf. Atmos. Rad.*, Madison, WI, 28 June–2 July, 21–24.

Minnis, P., and Couthors, 2002: Seasonal and diurnal variations of cloud properties derived for CERES from VIRS and MODIS data. *Proc. 11th AMS Conf. Atmos. Rad.*, Ogden, UT, 3–7 June, 20–23.

Poore, K., J. Wang, and W. B. Rossow, 1995: Cloud layer thicknesses from a combination of surface and upper-air observations. *J. Climate*, **8**, 550–568.

Randall, D. A., Harshvardhan, D. A. Dazlich, and T. G. Corsetti, 1989: Interactions among radiation, convection, and large-scale dynamics in a general circulation model. *J. Atmos. Sci.*, **46**, 1943–1970.

Rossow, W. B., and R. A. Schiffer, 1999: Advances in understanding clouds from ISCCP. *Bull. Amer. Meteor. Soc.*, **80**, 2261–2287.

Slingo, A., and J. M. Slingo, 1988: The response of a general circulation model to cloud longwave radiative forcing. I: Introduction and initial experiments. *Quart. J. Roy. Meteor. Soc.*, **114**, 1027–1062.

Slingo, J. M., and A. Slingo, 1991: The response of a general circulation model to cloud longwave radiative forcing. II: Further studies. *Quart. J. Roy. Meteor. Soc.*, **117**, 333–364.

Tian, L., and J. A. Curry, 1989: Cloud overlap statistics. *J. Geophys. Res.*, **94**, 9925–9935.

Wang, J., and W. B. Rossow, 1995: Determination of cloud vertical structure from upper-air observations. *J. Appl. Meteor.*, **34**, 2243–2258.

Wang, J., and W. B. Rossow, 1998: Effects of cloud vertical structure on atmospheric circulation in the GISS GCM. *J. Climate*, **11**, 3010–3029.

Wang, J., W. B. Rossow, T. Uttal, and M. Rozendaal, 1999: Variability of cloud vertical structure during ASTEX observed from a combination of rawinsonde, radar, ceilometer, and satellite. *Mon. Wea. Rev.*, **127**, 2484–2502.

Wang, J., W. B. Rossow, and Y. Zhang, 2000: Cloud vertical structure and its variations from a 20-yr global rawinsonde dataset. *J. Climate*, **13**, 3041–3056.

Warren, S. G., C. J. Hahn, and J. London, 1985: Simultaneous occurrence of different cloud types. *J. Climate Appl. Meteor.*, **24**, 658–667.

Warren, S. G., C. J. Hahn, J. London, R. M. Chervin, and R. L. Jenne, 1988: Global distribution of total cloud cover and cloud type amounts over ocean, NCAR Tech. Note, NCAR/TN-31 7+STR, 42 pp., plus 170 maps.

Weng, F., and N. C. Grody, 2000: Retrieval of ice cloud parameters using a microwave imaging radiometer. *J. Atmos. Sci.*, **57**, 1069–1081.

Wentz, F. J., 1998: Algorithm Theoretical Basis Document (ATBD): AMSR Ocean Algorithm, RSS Tech. Rep. 110398, Remote Sensing System, Santa Rosa, Canada.

Wielicki, B. A., R. D. Cess, M. D. King, D. A. Randall, and E. F. Harrison, 1995: Mission to planet earth: Role of clouds and radiation in climate. *Bull. Amer. Meteor. Soc.*, **76**, 2125–2153.

Zhao, L., and F. Weng, 2002: Retrieval of ice cloud parameters using the advanced microwave sounding unit. *J. Appl. Meteor.*, **41**, 384–395.